PIV: Direct Cross-Correlation compared with FFT-based Cross-Correlation

Oliver Pust

Department of Fluid Mechanics, Faculty of Mechanical Engineering
University of the Federal Armed Forces Hamburg, D–22039 Hamburg, Germany

1 Introduction

Particle Image Velocimetry (PIV) has become widely accepted as a reliable field measurement technique for the determination of velocity fields in the recent years. It has spread from research laboratories towards industrial applications. Several companies sell integrated turn-key systems. The principle of PIV is based on the comparison of two (or more) subsequent images of illuminated tracer particles which are assumed to follow the flow true-fully. The displacement that can be estimated by different means and the time separation between the images give the velocity information for a small subregion of the whole imaged area. Almost all algorithms for the estimation of the displacement of a group of tracer particles use cross-correlation techniques. For the sake of computational speed most authors and especially vendors of PIV-systems implement the cross-correlation-function by means of the discrete Fast-Fourier-Transform (FFT). Although this implementation has some drawbacks concerning flexibility and the accuracy of the computed velocity little or nothing is put down in literature about this conflict by the respective authors. The present article wants to draw the attention of developers and users of PIV-systems towards this aspect of image interrogation. This is not done by a theoretical or mathematical approach but by examples taken from the author's recent research.

2 Particle image interrogation methods

The idea of PIV is based on *Laser Speckle* measurement techniques developed in solid mechanics for the determination of surface roughness, vibration or deformation. Although there are distinctive differences between these techniques and flow velocity measurements, this is the reason why PIV was referred to as *Laser Speckle Velocimetry* in the early eighties.[1] Today it is common to distinguish between three methods of particle image interrogation, depending on the particle image density:

- Particle Tracking Velocimetry (PTV) for low image density,
- Particle Image Velocimetry (PIV) for medium image density and
- Laser Speckle Velocimetry (LSV) for high image density.

In the context of this article only the case of medium image density is taken into account as it is the most common mode of operation. Some authors suggested new terms for PIV, e. g. *Correlation Image Velocimetry (CIV)* as FINCHAM in [2]. In the authors opinion this leads to an unnecessary restriction as there are other methods of particle image interrogation that do not use correlation methods which search for the greatest correspondence between two signals. For example, a new method that searches for the smallest difference between two signals was proposed as the *Mean Quadratic Difference (MQD)* method by GUI and MERZKIRCH in [5]. This new promising method will also be taken into account for the following comparison.

Nevertheless, the focus of this article is put onto interrogation techniques that use correlation algorithms—and to be more specific only onto the case of two subsequent illuminations of the tracer particle pattern imaged

---

[1] See [11] for further information on this topic and [3], [4] for the development of PIV.

on two different frames. The usual method for the evaluation of two images separated by a small finite time step—each with only one illumination of the seeded flow—is called cross-correlation[2]. The cross-correlation function for two discretely sampled images (as they are the output of widely used CCD-cameras) is defined as:

$$\Phi_{fg}(m,n) = \sum_i \sum_j f(i,j) \times g(i+m,j+n) \tag{1}$$

with $f(i,j)$ and $g(i,j)$ denoting the image intensity distribution of the first and second image, m and n the pixel offset between the two images and $\Phi_{fg}(m,n)$ the cross-correlation function. Regarding that several thousand velocity vectors can be computed from one single pair of images the computational effort is enormous. Given the size of a square interrogation area N, a number of operations of the order of N^4 have to be computed. That is the main (and only) reason for introducing the *Fast Fourier Transform (FFT)* into the cross-correlation process. The computational effort is reduced to the $O[N^2 \ln N]$ which means a considerable speed-up of the evaluation process and that was necessary for the acceptance of PIV a few years ago when even workstations were not fast enough to compute the cross-correlation function directly within a reasonable time-scale. In the society of PIV this *implementation* of the cross-correlation function by the means of the FFT has been internalized by such a degree that one may read that PIV recordings are evaluated by using the FFT (See [13], [14] [15], [8], [9] for example.).

Some aspects of using FFT-based cross-correlation (FFT-CC) instead of direct cross-correlation (D-CC) are not mentioned or neglected too often: while the discrete cross-correlation function is well defined for finite regions (see equation 1) and therefore perfectly suited for the interrogation of finite sub-samples of PIV recordings, the FFT is well defined only for infinite domains. In order to apply the FFT the finite domain has to be extended to an infinite domain. The question how to do this adequately has to be handled with special care. Another limitation of the FFT is that—to be computationally efficient—the two sub-samples have to be of square and equal size and furthermore the size has to be a power of two (e. g. 16×16, 32×32 or 64×64). That may result in a loss of spatial resolution when N has to be selected larger than the maximum velocity would require to achieve a sufficient signal to noise ratio (SNR). Other problems that have to be dealt with are described in [10]. The effort that has to be taken to prevent FFT-caused artifacts is considerable and—as the results shown later suggest—is often futile or avoided. To the author's best knowledge the only other work that is devoted to evade the drawbacks of the FFT-CC can be found in [12], while several particle image interrogation methods are compared in [1] and [6]. As an example of a well implemented FFT-based cross-correlation algorithm, the PIV software package *pivware* by JERRY WESTERWEEL is used.[3] J. WESTERWEEL provided binaries of his code and assured that all possible means to avoid the drawbacks of the FFT-CC have been implemented.

3 Numerical implementation of the direct cross-correlation function

For the purpose of comparing the two cross-correlation methods the D-CC is modified in several ways to achieve the qualitatively best possible results:

- the size of the second sub-image is selected in such a way that—even with the maximal offset between the two sub-images applied— the edges of the first sub-image do not extend over the edges of the second sub-image,
- the average intensities of the sub-images $\bar{f}$ and $\bar{g}$ are computed and subtracted from the individual intensity values if these are greater than the average intensity; if the individual intensity values are smaller than the average intensity they are set equal to zero,
- the cross-correlation function is normalized suitably; the result is the cross-correlation coefficient function $\phi_{fg}(m,n)$ as shown in equation 2.

---

2 Details on the evaluation process can be found in [17], [7], [19]
3 The author wants to express his gratitude to JERRY WESTERWEEL for providing his software.

$$\phi_{fg}(m,n) = \frac{\sum_i \sum_j \left[f(i,j) - \bar{f} \right] \times \left[g(i+m,j+n) - \bar{g}(m,n) \right]}{\sqrt{\sum_i \sum_j \left[f(i,j) - \bar{f} \right]^2 \times \sum_i \sum_j \left[g(i,j) - \bar{g}(m,n) \right]^2}} \qquad (2)$$

It should be mentioned that $\bar{f}$ and $\bar{g}$ have to be computed in a different way. While $\bar{f}$ may be computed only once before the correlation process, $\bar{g}$ must be computed individually each time a new pixel offset between the two sub-images is chosen in order to result in the average intensity at (m,n).

Further consideration and observation of the quality of the results suggest one more slight modification in the computation of the normalization coefficient:

$$\phi_{fg}(m,n) = \frac{\sum_i \sum_j \left[f(i,j) - \bar{f} \right] \times \left[g(i+m,j+n) - \bar{g}(m,n) \right]}{\sqrt{\sum_i \sum_j \left[f(i,j) - \bar{f} \right]^2 \times \sum_i \sum_j \left[g(i+m,j+n) - \bar{g}(m,n) \right]^2}} \qquad (3)$$

It is favorable to take the intensity value of g at the same position $(i+m, j+n)$ both in the numerator for the correlation process and in the denominator for the normalization process. Table 1 emphasizes the benefit of the normalization process itself. The percentage of outliers based on the application of a global filtering process is considerably smaller for the case of normalization applied.

Table 1: Percentage of outliers for direct cross correlation (computed from the velocity fields of figure 4)

no normalization applied	4,23%
normalization applied	1,48%

4   Description of the evaluation parameters

Though it would be possible to apply non square interrogation areas using D-CC to take into account the dominant horizontal velocity of the investigated flow field[4], the interrogation size was set to 32×32 allowing direct comparison with the results of the FFT-based cross-correlation. In each case an overlap of 50% in both directions was chosen. In addition to the principle consideration of FFT-CC and D-CC the influence of the chosen peak-finder was also investigated for the case of FFT-CC because the application of the parabolic peak-finder can still be found in available software. Furthermore for its growing propagation an adaptive FFT-based cross-correlation algorithm was considered, too. Here in the first step the interrogation size was set to 32×32 with 50% overlap, while in the second step the interrogation size was set to 16×16 with no overlap resulting in a vector map with an identical number of vectors at the same positions as in the

Figure 1: Enlarged 32×32 particle image sample

other three cases. Some parameters of the interrogated images may be of some interest: the average particle image diameter is ≈ 2.2 pixel and the image density is ≈ 23 (see figure 1).

5   Results

The results of the different evaluations are presented in three ways: Figure 3 shows profiles of the horizontal velocity across the height of the channel, in figure 4 one can find scatter plots of all the velocity vectors that have been computed, finally histograms of the horizontal velocity components are depicted in figure 5. In contrast to these instantaneous vector maps figures 6, 7 and 8 show the same visualizations for vector maps

---

4   The images were taken in the steady inflow of the water channel that is described in detail in [16].

that have been averaged from ten realizations of the flow field. In the captions of the figures the abbreviations have to be read as: A–adaptive algorithm, NWF–second sub-image of the same size as first sub-image, WF–second sub-image of greater size than first sub-image, N–cross-correlation function is normalized, NN–cross-correlation function is not normalized, PPF–parabolic peak fit, GPF–Gaussian peak fit.

An effect that is often overlooked when viewing vector maps or velocity profiles of turbulent flow fields is the so called *peak locking effect*.[5] It describes the fact that velocities tend towards integer pixel values. Mostly this effect is attributed to particle image diameters that are only of the size of a pixel. The error becomes minimal for a particle image diameter of ≈ 2.[6]

Laminar flow fields at low Reynolds number are expected to show smooth velocity profiles without sharp bends. As the velocity profile in the water channel for these experiments is known from LDV measurements[7], it is surprising to find profiles with sharp bends at integer velocity values and a maximum plateau whose value is close to 4 pixel/32 ms. Comparing the two profiles resulting from the standard FFT-CC algorithm it may surprise that there is only little difference between the parabolic peak fit and the Gaussian peak fit (see figures 3(a) and 3(b)). The roughness of the profile becomes even worse for the adaptive algorithm although the particle image density for a 16×16 interrogation area is greater than 5. The optimized D-CC algorithm clearly performs better. There are no remarkable sharp bends, the curvature of the profile is more pronounced and in addition the maximum value is ≈ 0.15 pixel/32 ms higher. The profile of the MQD method looks much the same as the ones of the FFT-CC: there are no noticeable improvements. *Pivware* results are similar to the D-CC results although the roughness of the profile is larger.

The peak locking effect becomes evident in figure 4(a)–(c) and 4(f): the dots are clustered at the grid points while in figure 4(d) and 4(e) the dots are distributed more evenly within the velocity domain. Other useful means to prove the peak locking effect are histograms of the velocity components. The histograms in figure 5(a)–(c) show a strong accumulation around the integer values 1, 2, 3 and 5 which indicate the peak locking effect. The high peak around the value 4 cannot be called peak locking as it obviously represents the dominating velocity range in the flow field. In figure 5(d) the accumulation is much smaller and in addition it has to be noted that the maximum count is just 300 in contrast to 500 for the other histograms. Again the MQD method (figure 5(f)) shows no advantage over the FFT-CC: the peak locking is prominent in both cases. The histogram of the optimized FFT-CC (figure 5(e)) is smoother than for the not optimized FFT-CC, but still there are high peaks at 1 and 2.

The results of the MQD method need further explanation. One might expect from the work in [6] that the MQD method should at least reach the quality of the D-CC or perform even better. As GUI and MERZKIRCH explain the MQD method is "in principle a tracking of patterns of particle images" and therefore is very sensitive to underlying (systematic) image noise. For their comparison the authors used artificially generated particle images where only the particle positions have been taken from real recordings. Influences during the recording of real images like different light sheet intensity between first and second image or characteristics of the CCD chip are not considered. The effect that can be observed in figure 2 may explain an aspect of the problem. The camera that recorded that sample is an often used Kodak ES 1.0. It utilizes two A/D converters to read out the pixel lines. As there are always small deviations between

Figure 2: Enlarged 32×32 image sample

the conversion efficiency of the two converters, even a previously uniform image intensity distribution will show horizontal lines of different gray values after having been read out. These horizontal lines represent an artificial pixel pattern and the MQD method tracks this pattern with an apparent vertical integer displacement. As this explains only vertical peak locking further research is necessary in that respect.

---

[5] The reason that peak locking in turbulent flow fields is not that prominent may be that it is the nature of turbulence that mean velocities are superimposed by random spatial and temporal fluctuations.

[6] The peak locking effect is explained in detail in [18], [10].

[7] See figure 3(a) in [16].

One might think that averaging several vector maps could eliminate the peak locking but that is not the fact. Several authors explain peak locking as a systematical error and while averaging will eliminate random errors the peak locking becomes more dominant. This statement is underlined by figures 6, 7 and 8. The histograms for the FFT cases and the MQD method do not change notably but the histogram for the D-CC case looks a little smoother than the not averaged one.

6 Conclusions

This article has the aim to make more sensitive for the differences between the algorithms that are used for the evaluation of particle image recordings. It has been shown that representative FFT-CC algorithms and the MQD method perform poorer than an optimized D-CC algorithm. Moreover, there is evidence that peak locking is not only caused by small particle images but also influenced by the algorithm in question. For FFT-CC the choice of the peak fit is not very important while the investigations for D-CC have made clear that the Gaussian peak fit performs better. Adaptive FFT-CC schemes, that seem to be promising, may enlarge spatial resolution but do not enhance the quality of the results. In D-CC there is no need for adaptive schemes as the reduction of the interrogation size can be done in a single step because the first sub-image always fits completely into the second (larger) sub-image. The only justification for FFT-CC is its higher computational speed. If the results of measurements are to be controlled in near real time for the purpose of aligning the PIV-system, the application of FFT may still be favorable although the correlation of ≈ 4000 vectors takes about 20 s on a SUN Ultra 5 with 270 MHz. Deciding between D-CC and optimized FFT-CC means weighing the advantage of the slightly better results of the D-CC against its disadvantageous higher computational time and the effort to avoid the drawbacks of the FFT-CC while still using the FFT. There are two final recommendations:

1. use direct cross-correlation based algorithms if the results have to be as exact as possible,
2. assess the quality of particle image interrogation methods not only by evaluating synthetic images but also by using images that have been recorded under real conditions in the laboratory.

References

[1] FEI, R. ; GUI, L. ; MERZKIRCH, W. : Vergleichende Untersuchungen von korrelativen PIV-Auswerteverfahren. In: *Lasermethoden in der Strömungsmeßtechnik*, 1998, pp. 35.1–35.8 2

[2] FINCHAM, A. M. ; SPEDDING, G. R.: Low cost, high resolution DPIV for measurement of turbulent fluid flow. In: *Experiments in Fluids* 23 (1997), pp. 449–462 1

[3] GRANT, I. : Particle image velocimetry: a review. In: *Proceedings of the Institution of Mechanical Engineers* Vol. 211 C, 1997, pp. 55–76 1

[4] GRAY, C. ; GREATED, C. A.: Evolution of the partial image velocimetry measuring technique. In: *Strain* 31 (1995), No. 1, pp. 3–8 1

[5] GUI, L. ; MERZKIRCH, W. : A method of tracking ensembles of particle images. In: *Experiments in Fluids* 21 (1996), pp. 465–468 1

[6] GUI, L. ; MERZKIRCH, W. : A comparitive study of the MQD method and several correlation-based PIV evaluation algorithms. In: *Experiments in Fluids* 28 (2000), pp. 36–44 2, 4

[7] KEANE, R. D. ; ADRIAN, R. J.: Theory of cross-correlation analysis of PIV images. In: *Applied Scientific Research* 49 (1992), pp. 191–215 2

[8] MEINHART, C. D. ; PRASAD, A. K. ; ADRIAN, R. J.: A parallel digital processor system for particle image velocimetry. In: *Measurement Science & Technology* 4 (1993), pp. 619–626 2

[9]   PRASAD, A. K. ; ADRIAN, R. J. ; LANDRETH, C. C. ; OFFUTT, P. W.:   Effect of resolution on the speed and accuracy of particle image velocimetry interrogation. In: *Experiments in Fluids* 13 (1992), pp. 105–116 2

[10] RAFFEL, M. ; WILLERT, C. E. ; KOMPENHANS, J. :   *Particle image velocimetry: a practical guide.* Berlin : Springer, 1998 2, 4

[11] RIETHMULLER, M. L. (Editor):   *Particle Image Velocimetry – Lecture Series 1996-03.* Rhode Saint Genèse : von Karman Institute for Fluid Dynamics, 1996 1

[12] RONNEBERGER, O. ; RAFFEL, M. ; KOMPENHANS, J. :   Advanced Evaluation Algorithms for Standard and Dual Plane Particle Image Velocimetry. In: *Proceedings of the Ninth International Symposium on Applications of Laser Techniques to Fluid Mechanics, 13–16 July 1998, Lisbon, Portugal*, 1998, pp. 10.1.1–10.1.8 2

[13] SCARANO, F. ; RIETHMULLER, M. L.:   Iterative multigrid approach in PIV image processing with discrete window offset. In: *Experiments in Fluids* 26 (1999), pp. 513–523 2

[14] SHIANG, A. H. ; LIN, J. C. ; ÖZTEKIN, A. ; ROCKWELL, D. :   Viscoelastic flow around a confined circular cylinder: measurements using high-image-density particle image velocimetry. In: *Journal of Non-Newtonian Fluid Mechanics* 73 (1997), pp. 29–49 2

[15] SORIA, J. :   An Investigation of the Near Wake of a Circular Cylinder Using a Video-Based Digital Cross-Correlation Particle Image Velocimetry Technique. In: *Experimental Thermal and Fluid Science* 12 (1996), pp. 221–233 2

[16] STENZEL, O. ; LUND, C. :   Laser Doppler Velocimetry (LDV) and Particle Image Velocimetry (PIV) Measurements of the Time Dependent Flow behind a Circular Cylinder and Comparison with Results Obtained by Numerical Simulation. In: *Proceedings of the 9th International Symposium on Applications of Laser Techniques to Fluid Mechanics. Lisbon, Portugal*, 1998, pp. 2.4.1–2.4.8 3, 4

[17] WESTERWEEL, J. :   *Digital Particle Image Velocimetry: Theory and Application.* Delft University Press, Delft, Delft University of Technology, Thesis, 1993 2

[18] WESTERWEEL, J. :   Effect of Sensor Geometry on the Performance of PIV Interrogation. In: *Proceedings of the Ninth International Symposium on Applications of Laser Techniques to Fluid Mechanics, 13–16 July 1998, Lisbon, Portugal*, 1998, pp. 1.2.1–1.2.8 4

[19] WILLERT, C. E. ; GHARIB, M. :   Digital particle image velocimetry. In: *Experiments in Fluids* 10 (1991), pp. 181–193 2
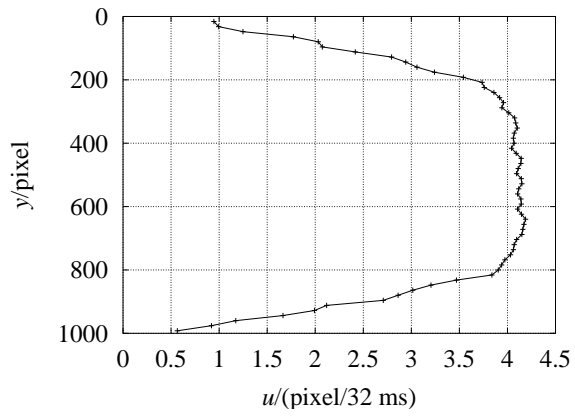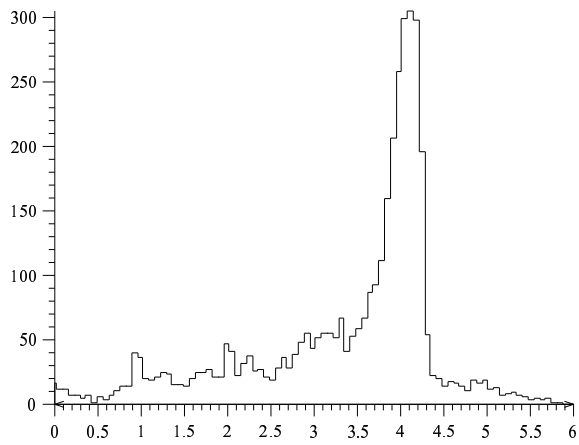
(a) FFT-NWF-NN-PPF
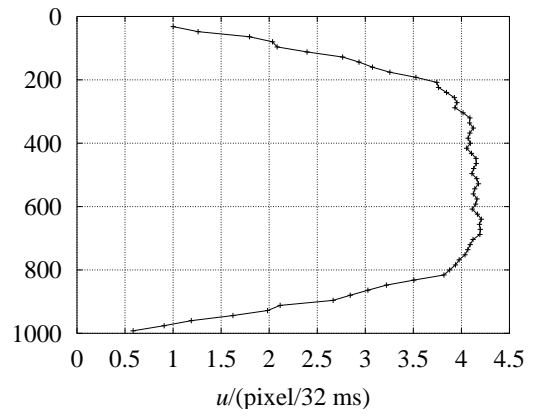
(b) FFT-NWF-NN-GPF
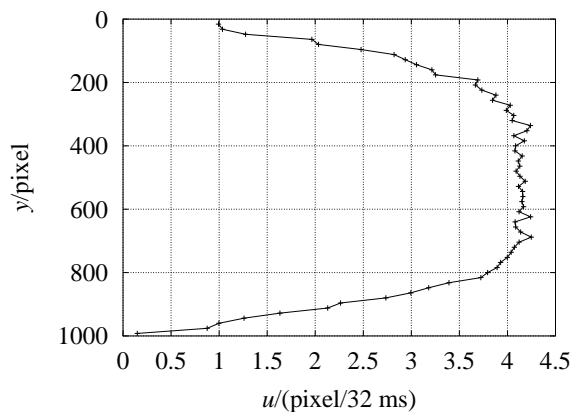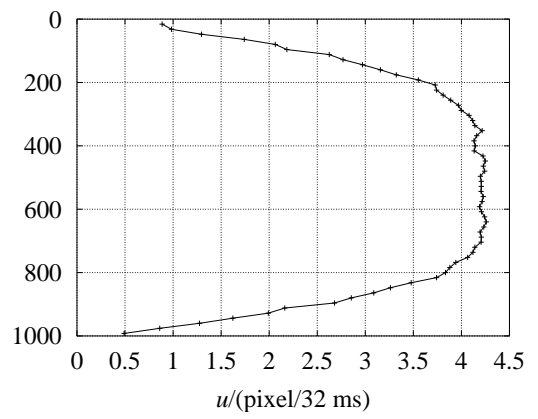
(c) FFT-A-NWF-NN-GPF
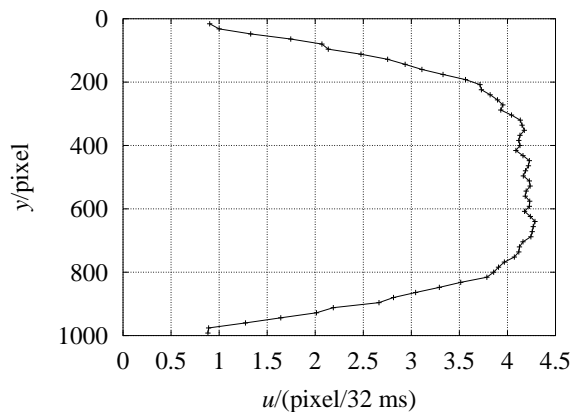
(d) D-CC-WF-N-GPF
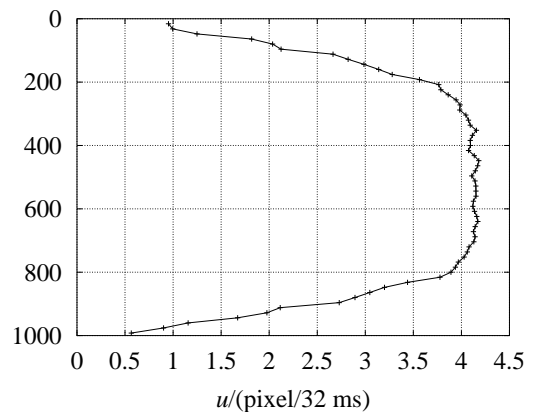
(e) FFT (Westerweel)

(f) MQD method

Figure 3: Horizontal velocity profiles
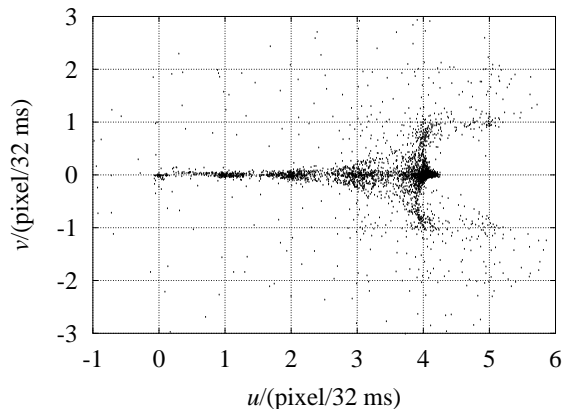
(a) FFT-NWF-NN-PPF
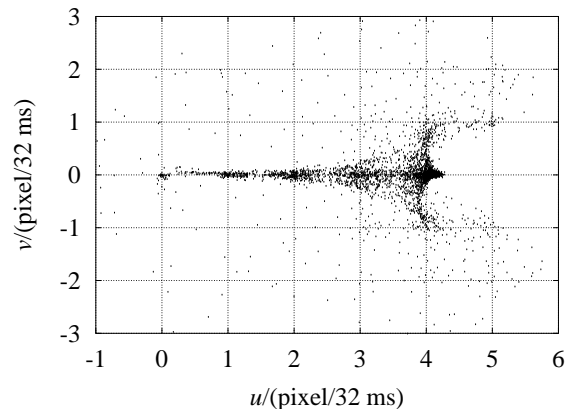
(b) FFT-NWF-NN-GPF
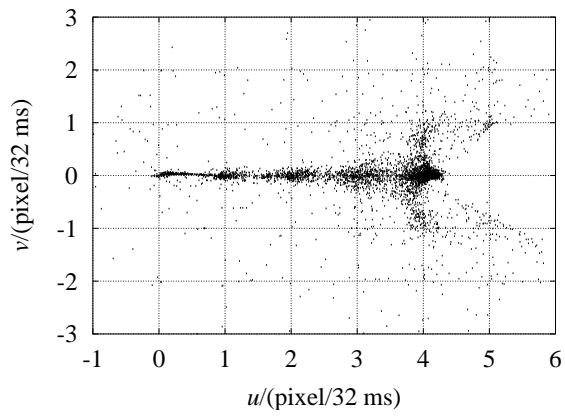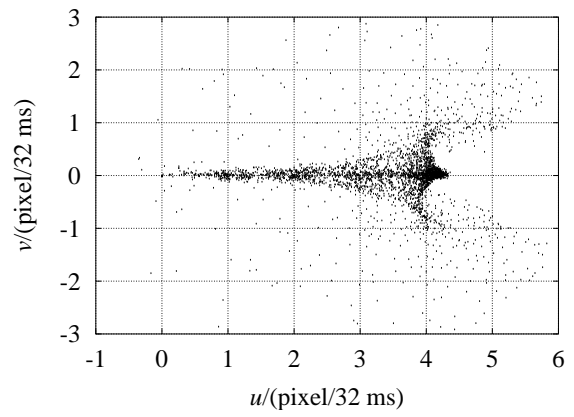
(c) FFT-A-NWF-NN-GPF
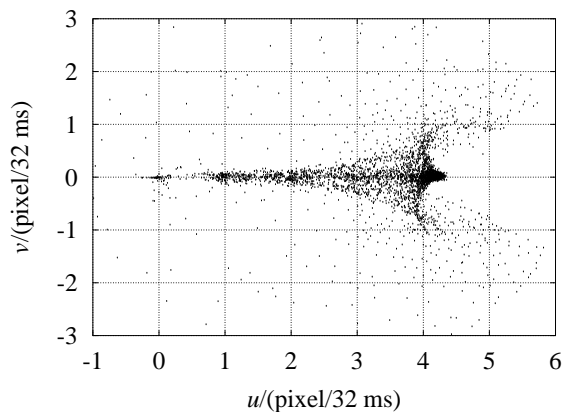
(d) D-CC-WF-N-GPF
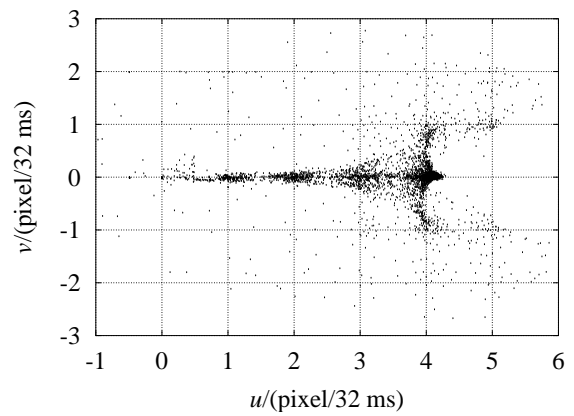
(e) FFT (Westerweel)

(f) MQD method

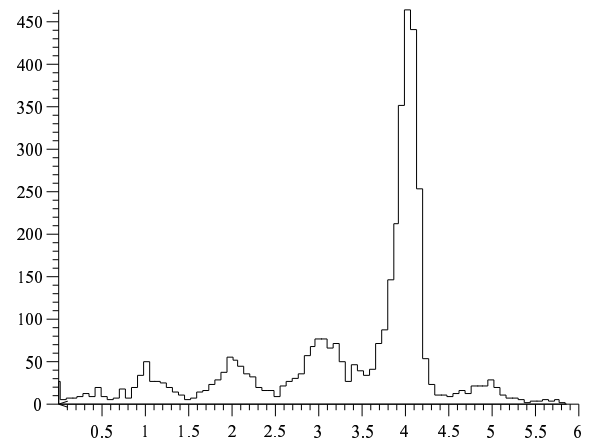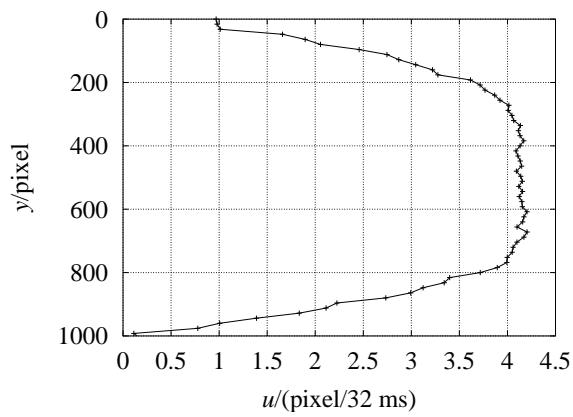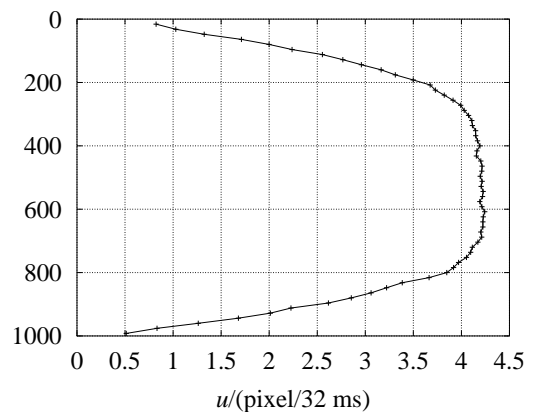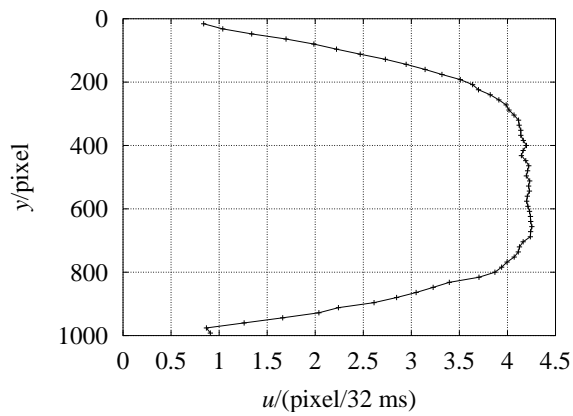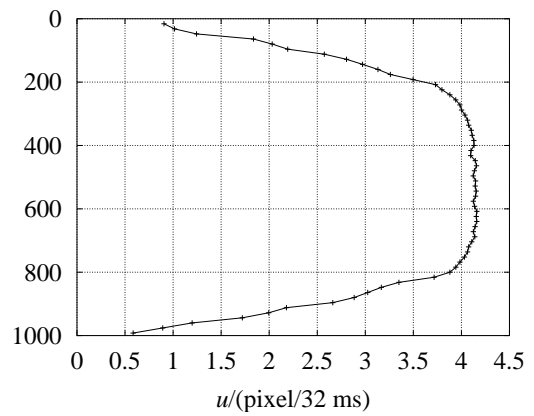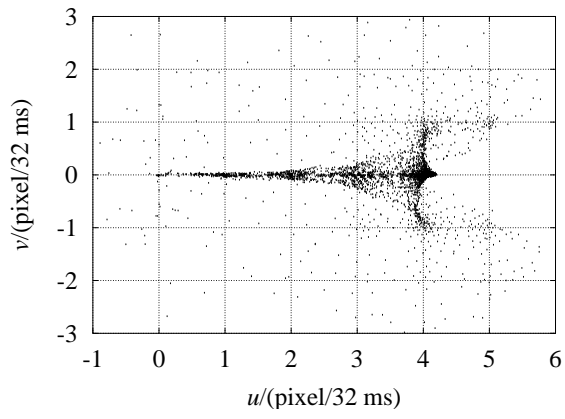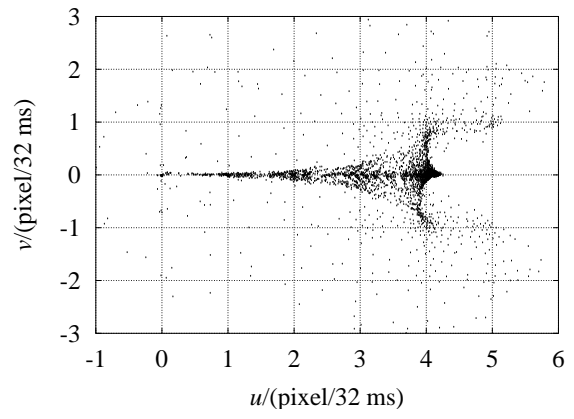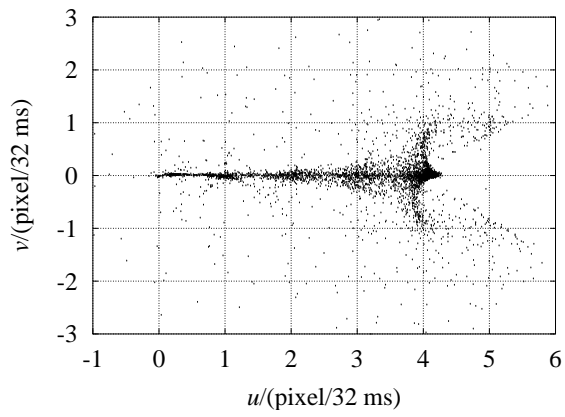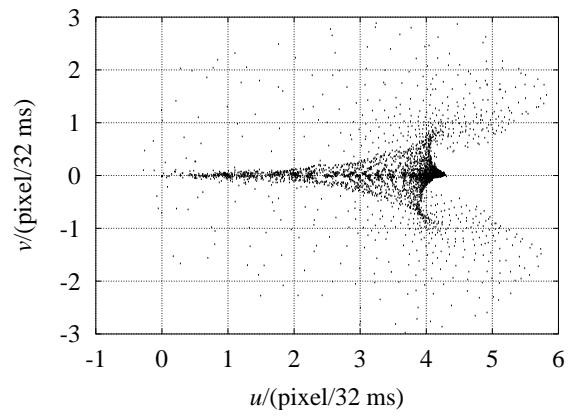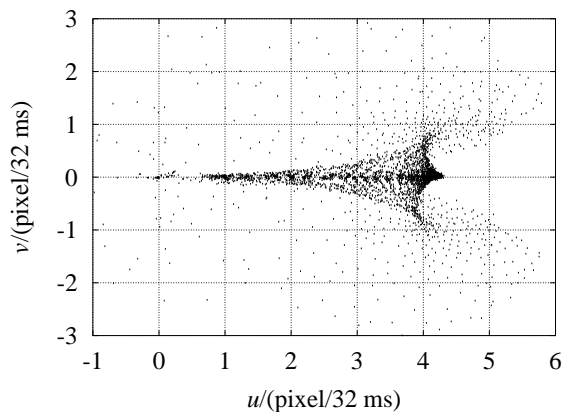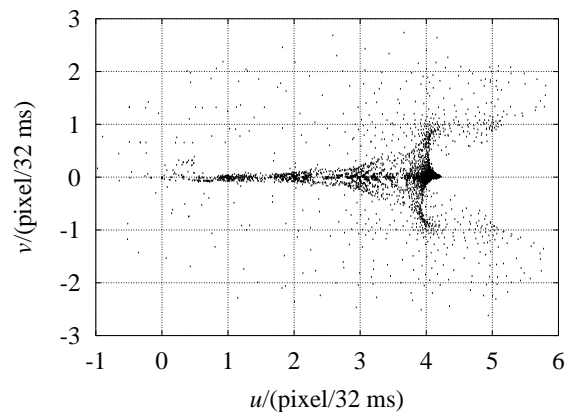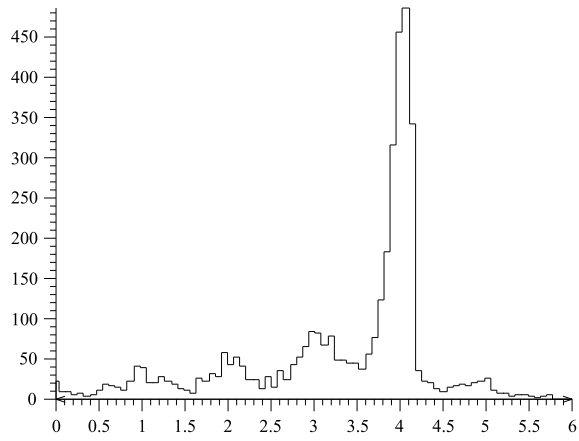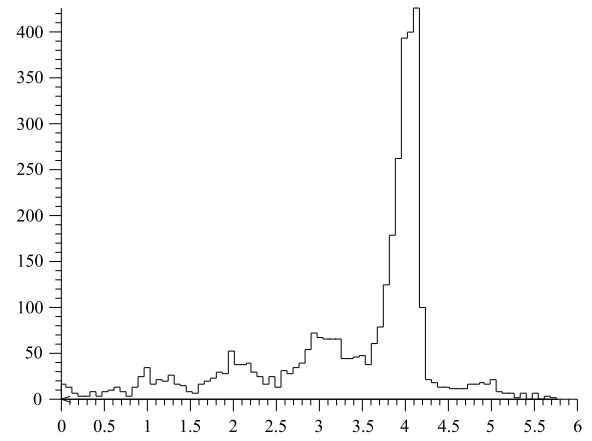**Figure 4:** Scatter plot of the velocities
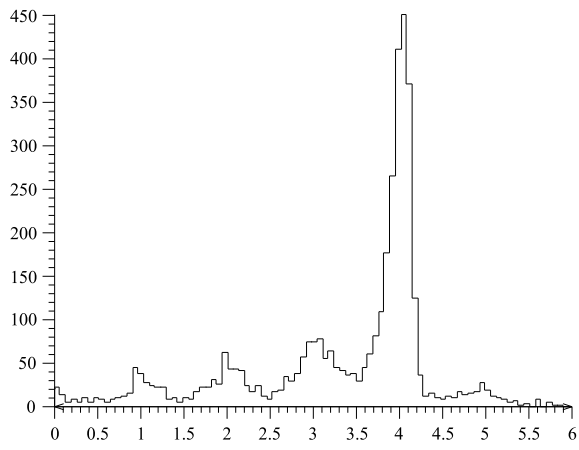
(a) FFT-NWF-NN-PPF
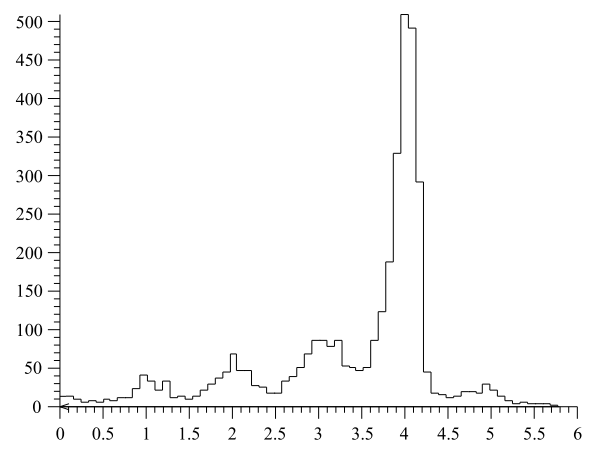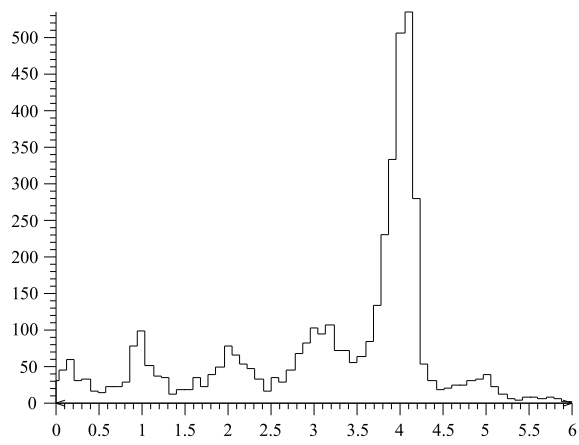
(b) FFT-NWF-NN-GPF
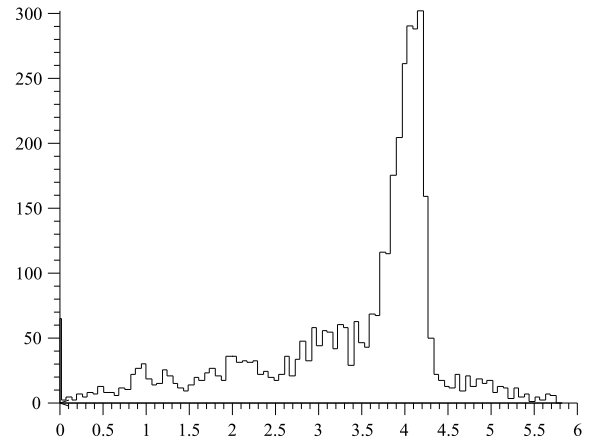
(c) FFT-A-NWF-NN-GPF

(d) D-CC-WF-N-GPF

(e) FFT (Westerweel)

(f) MQD method

Figure 5: Histograms of the horizontal velocity component
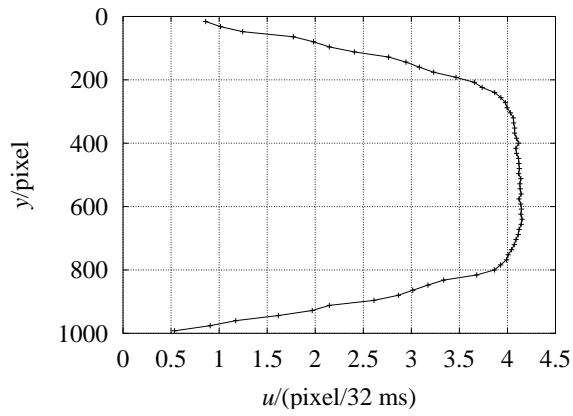
(a) FFT-NWF-NN-PPF
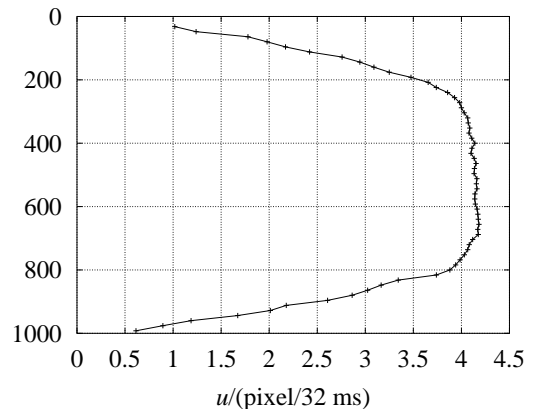
(b) FFT-NWF-NN-GPF

(c) FFT-A-NWF-NN-GPF

(d) D-CC-WF-N-GPF

(e) FFT (Westerweel)

(f) MQD method

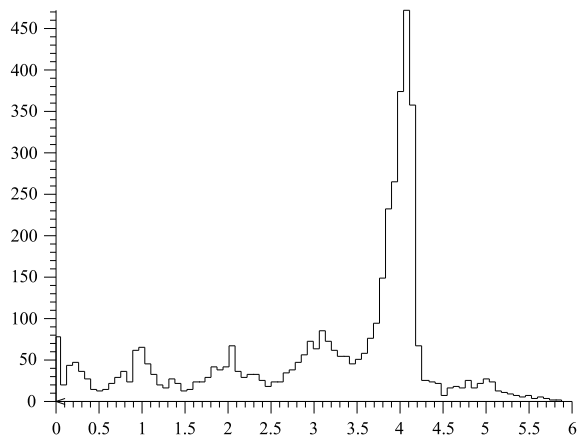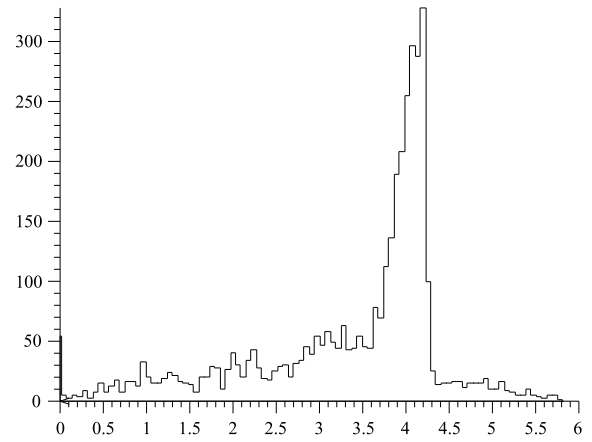**Figure 6:** Averaged horizontal velocity profiles

Figure 7: Scatter plot of the averaged velocities
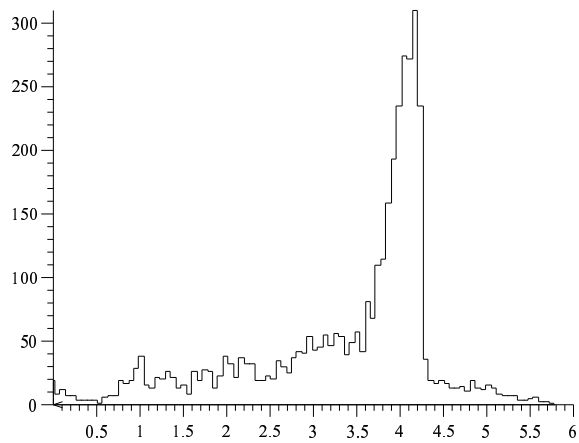
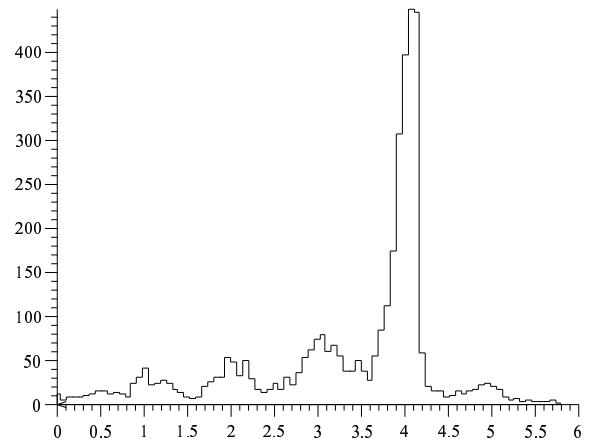(a) FFT-NWF-NN-PPF

(b) FFT-NWF-NN-GPF

(c) FFT-A-NWF-NN-GPF

(d) D-CC-WF-N-GPF

(e) FFT (Westerweel)

(f) MQD method

Figure 8: Histograms of the averaged horizontal velocity component